Numerical study on freely floating vertical cylinders by fully nonlinear three-dimensional potential-flow numerical wave tank

Sung-Jae Kim, Moo-Hyun Kim
Department of ocean engineering, Texas A&M university, College station, Texas, USA
(email : sungjaekim1001@gmail.com, m-kim3@tamu.edu)

1. Introduction

The estimation of wave-body interaction with nonlinear waves is one of the remaining challenging in this research area. In particular, in case of floating renewable energy converting devices such as floating wind turbines and wave energy converters, it should be operated in highly nonlinear waves because the wave energy is proportional to the square of wave amplitude. Numerical wave tank is one of useful tools to simulate wave-body interaction in nonlinear waves and uniform current. Since it expresses physical wave tank test numerically, it has good potential to simulate various hydrodynamic phenomena such as wave-wave interaction, wave-slope bottom interaction, wave-current-body interaction, hydroelasticity in nonlinear waves and so on. In this study, the fully nonlinear potential-flow numerical wave tank was used to evaluate nonlinear excitation force acting on the body and wave-body interaction for a vertical circular cylinder. And then, the uniform current effect is estimated by a three-dimensional potential-flow numerical wave tank.

2. Numerical wave tank

A three-dimensional potential-flow numerical wave tank (3D-NWT) is one of useful tools to estimate high-order excitation force acting on the on/offshore structures and simulate nonlinear wave-body interaction in waves with uniform current. It is based on potential flow theory and boundary element method (BEM). To reduce computational demand, image sources are located with respect to mean water level and flat bottom and the fluid domain is assumed to be x-axis symmetry. Governing equation can be presented as Laplace equation and total potential can be expressed as Eq. (1) including the effect of uniform current flow. Based on Green's second identity, boundary integral equation can be established as Eq. (2).

$$\tilde{\phi}(x,y,z,t) = \phi(x,y,z,t) + Ux \tag{1}$$

$$\alpha_s \phi = \int_S \left(G \frac{\partial \phi}{\partial n} - \phi \frac{\partial G}{\partial n} \right) dS \tag{2}$$

$$G = \frac{1}{r_1} + \frac{1}{r_2} + \frac{1}{r_3} + \frac{1}{r_4} \tag{3}$$

where, U and α_s are velocity of uniform current flow and solid angle. G is Green function, which is expressed as the three-dimensional Rankine source. Eqs. (4)~(6) show boundary conditions at each boundary surface.

$$\frac{\partial \phi}{\partial n} = \vec{V} \cdot \vec{n} - U n_x \quad \text{on} \quad S_B \tag{4}$$

$$\frac{\delta \eta}{\delta t} = \frac{\partial \phi}{\partial z} - (\nabla \phi - \vec{v}) \cdot \nabla \eta - U \frac{\partial \eta}{\partial x} - \mu_1 \eta \quad \text{on} \quad S_F \tag{5}$$

$$\frac{\delta \phi}{\delta t} = -g\eta - \frac{1}{2} |\nabla \phi|^2 + \vec{v} \cdot \nabla \phi - U \frac{\partial \phi}{\partial x} - \mu_2 \frac{\partial \phi}{\partial n} \quad \text{on} \quad S_F \tag{6}$$

Where, $\vec{V}$, $\vec{n}$, η and $\vec{v}$ denote velocity vector of a rigid body, normal vector at each panel, wave elevation and particle velocity of the collocation point, respectively. S_B and S_F are wetted body surface and free-surface. In addition, inflow boundary surface (S_{in}) and side and back wall boundary surface (S_{wall}) are existing. The profiles of third order Stokes waves are fed at inflow boundary surface and the side and back wall boundary surface expressed as impermeable boundary condition ($\partial \phi / \partial n = 0$). In this study, $\vec{v}$ is defined according to types of the structures (i.e. semi-Lagrangian approach ($\vec{v} = (0, 0, \delta \eta / \delta t)$) for fixed structures, full-Lagrangian approach ($\vec{v} = \nabla^2 \phi + U n_x$) for floating structures). In 3D-NWT, the location of all calculation nodes is updated according to physical movement of free-surface and the structure

based on the MEL method. The last term of Eqs. (5) and (6) is artificial damping term to avoid reflected waves from side wall and end wall. μ_1 and μ_2 are artificial damping terms, which has a relation as $\mu_2 = k\mu_1$ (Koo and Kim, 2004). Fig. 1 shows overview of 3D-NWT. The checkered surface at free-surface is presented artificial damping zone. Hydrodynamic pressure acting on the structure can be presented as Eq. (7) based on Bernoulli equation. Equations of motion can be described as Eq. (8) and (9).

$$p = -\rho\left(gz + \frac{1}{2}|\nabla\phi|^2 + \frac{\partial\phi}{\partial t} + U\frac{\partial\phi}{\partial x} \right) \tag{7}$$

$$m\vec{a} = \vec{F} = \int_{S_B} p\vec{n}dS - W\delta_{i3} \tag{8}$$

$$I\ddot{\vec{\theta}} = \vec{M} = \int_{S_B} p(\vec{n}\times\vec{r})dS \tag{9}$$

Where, p, g, m, I and W are hydrodynamic pressure, gravitational acceleration, mass of a rigid body, moment of inertia of a rigid body and weight of rigid body, respectively. δ_{ij} is the Dirac delta function. In order to evaluate time derivatives of velocity potential, acceleration potential approach is adopted. It calculates the time derivative in acceleration field by solving additional boundary value problem to respect with the time derivatives of velocity potential (ϕ_t) which satisfies the Laplace equation. And, for convenience of calculation, the time derivative of velocity potential can be decomposed to seven components for which six components are from motions and the last component from velocity field. The detailed is in Koo and Kim (2004) and Kim and Koo (2019).

For the fully nonlinear time-domain analysis, the wetted body surface and free-surface are updated according to their physical movement at every time step. Firstly, we evaluate displacement of a rigid body and update location of all grids of the whole body according to its displacement. Then, the program estimates the intersection line between the body and free-surfaces by using the updated grids of the whole body, and the free-surface grids also updated from the previous time step. Besides, the Runge-Kutta fourth order time integration method is adopted for time marching and the liner systems of equations is solved by GMRES solver, which is well known iteration solver. We apply additional numerical schemes such as least square gradient reconstruction method, inverse distance weighting method, thin plate spline method. The detailed is in Kim and Koo (2019).

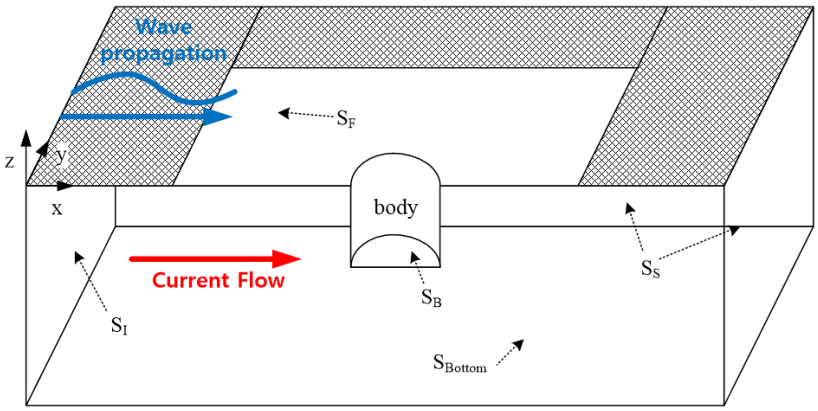

Fig. 1 Overview of three-dimensional numerical wave tank

3. Numerical Results

In this study, the author-developed NWT is utilized to evaluate high-order excitation force and nonlinear motions. Firstly, we solve diffraction problem without uniform current flow. Fig. (2) shows first order, second order and third order horizontal wave loads acting on a fixed vertical cylinder. The cylinder has draft-to-radius-ratio (d/R) of 1.0 and water depth is 10.0 times the draft. For comparison, additional numerical analysis was performed by commercial hydrodynamic frequency domain analysis software, WAMIT to obtain first order and second order excitation force. And third order triple frequency wave loads are compared with Teng and Kato (2002). They conducted numerical study based on the perturbation-based time domain analysis. They are in a good agreement. To obtain third order wave loads, even if perturbation-based time domain analysis needs somewhat complicated boundary conditions, in case of 3D-NWT, it is possible to estimate them by feeding third order Stokes waves at inflow boundary surface.

Next, numerical simulation was conducted to investigate hydrodynamic performance of a floating vertical cylinder without uniform current flow. It has draft-to-radius-ratio of 4.0, center of gravity (z_G / R) of -2.063 and pitch-roll radius of gyration (r_{yy} / R) of 0.853. And, water depth is set to 8.0 times the radius. The first order and second order motion RAOs were compared with the results of Moubayed and Williams (1994) as Fig. 3. They estimated motion RAOs by their own approaches based on the frequency domain perturbation method. Even though we already calculated three degrees of freedom (surge-heave-pitch), in this study, heave and pitch motion RAOs are only presented. The results of both the first order and the second order motion RAOs have a good agreement with published results. In addition, motion displacements were compared at kR =0.2 (Fig. 4) close to heave natural frequency. In this case, pitch motion amplitude was amplified at certain wave height condition (H / λ =1/392). Even if wave steepness is very mild, Mathieu-type instability occurs because of resonant heave motion. In fig. 4 (a), slowly varying heave motion envelope is observed as Haslum and Faltinsen (1999) because of small radiation damping. After $time / T$ =23, the pitch motion starts to be amplified with not wave period but pitch natural period. This kind of phenomena can be observed by using the fully nonlinear NWT.

Then, we investigated excitation wave loads on a fixed vertical cylinder with uniform flow. In Fig. 5, horizontal wave loads with uniform current flow. The body has the dimensionless draft (d / R) of 1.0 and water depth is same to the draft. Two different Froude number conditions (Fn) were considered. The results were compared with published results of Kim and Kim (1997). They are in a good agreement. It seems that x-axis of Fig. 5 is shifted due to variation of encounter frequency from wave-current interaction.

4. Conclusion

In this study, the developed fully nonlinear NWT is based on MEL method and acceleration potential approach. It was used for various numerical simulations such as a stationary body in waves, a freely floating body in waves and a stationary body in waves and current. The results were summarized as follow.

- High-order wave loads can be evaluated by the fully nonlinear NWT without complicated boundary condition which is needed in the perturbation method.
- Not only first and second order motion RAOs can be estimated well, but also Mathieu-type instability phenomena, which is expressed by conventionally frequency domain analysis or linear time domain analysis, can be observed through the fully nonlinear NWT.
- The current effect can be easily added in the fully nonlinear NWT, but reasonably.

Acknowledgement

References

Haslum, H.A & Faltinsen, O.M., 1999. Alternative shape of spar platforms for use in hostile areas, In: Offshore Tec. Conf. (OTC 10953), Houston, Texas, USA.

Kim, D.J. & Kim, M.H., 1997. Wave-Current Interaction with a Large Three-Dimensional Body by THOBEM, J. Ship Res., 41(4), 273-285.

Kim, S.J. & Koo, W., 2019. Development of a three-dimensional fully nonlinear potential numerical wave tank for a heaving buoy wave energy converter, Math. Prob. Eng., 2019, 5163597, 1-17

Koo,W. & Kim, M.H., 2004. Freely floating body simulation by a 2D fully nonlinear numerical wave tank, Ocean Eng., 31, 2011–2046.

Moubayed, W.I. & Williams, A.N., 1994. The second-order diffraction loads and associated motions of a freely floating cylindrical body in regular waves: an eigenfunction expansion approach, J. Fluids Struct., 8, 417-451.

Teng, B. & Kato, S., 2002. Third order wave force on axisymmetric bodies. Ocean Eng., 29, 815-843.

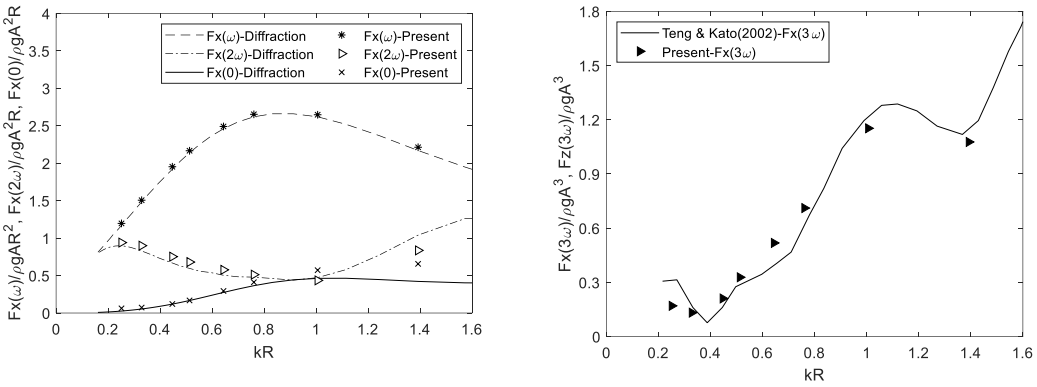

(a) First and second order wave loads (b) third order wave loads

Fig. 2 First order wave-frequency, second order mean-drift, second order double-frequency and third order triple-frequency horizontal wave loads

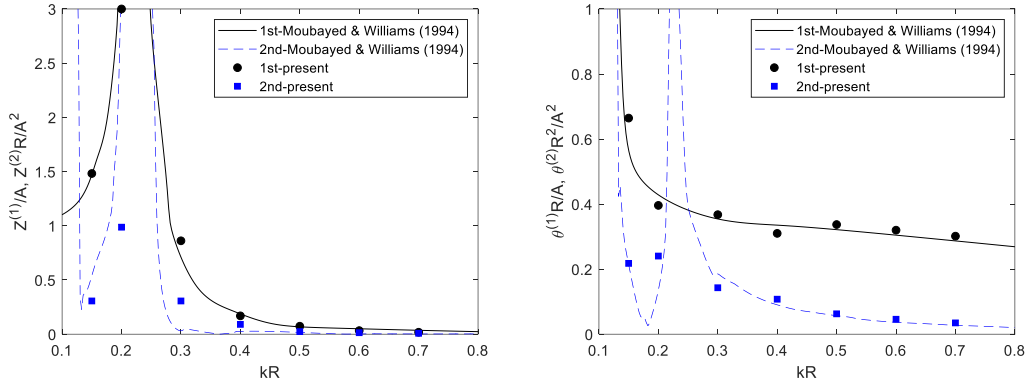

(a) Heave RAO (b) Pitch RAO

Fig. 3 First order and second order RAO for three degrees of freedom

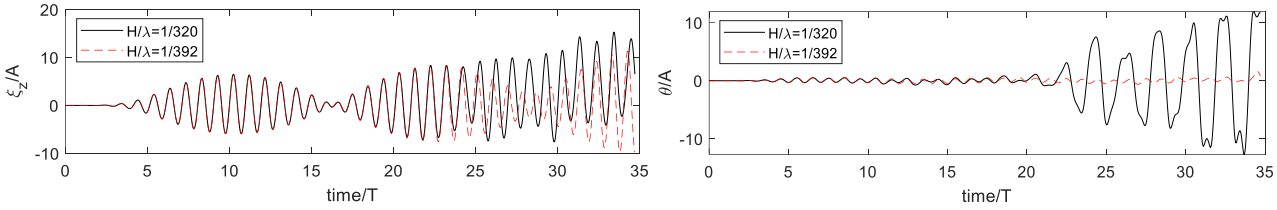

(a) Heave displacement (b) Pitch displacement

Fig. 4 Motion displacements of a floating cylindrical structure on various wave amplitude (kR =0.2, a: heave motion, b: pitch motion)

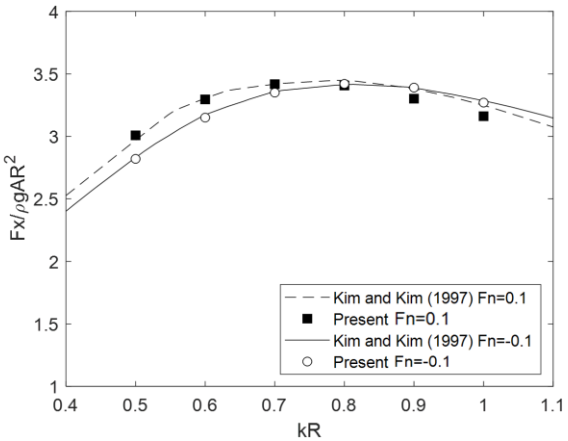

Fig. 5 Horizontal wave loads on a fixed vertical cylinder with waves and uniform current flow